PCCP

PAPER

View Article Online
View Journal | View Issue

Cite this: *Phys. Chem. Chem. Phys.*, 2016, **18**, 13941

The mechanism of the dielectric relaxation in water

Ivan Popov,[ab] Paul Ben Ishai,[a] Airat Khamzin[b] and Yuri Feldman*[a]

Received 3rd April 2016,
Accepted 28th April 2016

DOI: 10.1039/c6cp02195f

www.rsc.org/pccp

Although relating to the same system, the interpretations of the water spectra from Raman and Dielectric spectroscopy present independent pictures of the nature of water. We show that in the overlap region of the two methods it is possible to combine these views into a coherent concept of what drives the dynamic features of water. In this work, we develop the idea that the dielectric relaxation in water is driven by the migration of defects through the H-bond network, leading to a Debye-like peak in the lower frequencies. The deviation from the Debye law in the higher sub-THz frequencies is traced to a global fluctuation of the same H-bond network, clearly evident in the Raman Spectra. By incorporating these two views, a mathematical formalism is presented that can aptly explicate the dielectric spectra of liquid water.

Introduction

Water is an extensively studied subject as it plays an important role in life. In its liquid state it has numerous anomalous properties that significantly distinguish it from other simple liquids.[1] The most important of these are linked to the strong polarity of the water molecules[2–5] and their ability to establish an elastic hydrogen-bonded (H-bonded) network.[6] The complexity of water's properties has led to literally hundreds of theoretical and computational models for water.[7] The more famous and commonly used ones[8–13] succeed in describing various static features of water (temperature dependences of density, heat capacitance, static dielectric permittivity and so forth). However, these models cannot predict the correct dynamical properties of water and cannot adequately describe its dielectric and infrared spectra.[14] In turn, the investigation of water's dynamical behavior is an important prerequisite to the understanding of the role of water in various biological systems.

The collective dielectric response of water is usually measured using a variety of techniques, depending on the frequency region of interest. Nowadays, the development of broad band dielectric spectroscopy (BDS), which includes the Microwave range and THz region, together with the far infrared (FIR) spectroscopy enables the evaluation of continuous dielectric spectra over an extremely broad frequency band.[15] Fig. 1 presents the wide dielectric spectra of water at 20 °C up to 17 THz. The main dielectric relaxation peak obeys the Debye law up to a few tens of gigahertz,

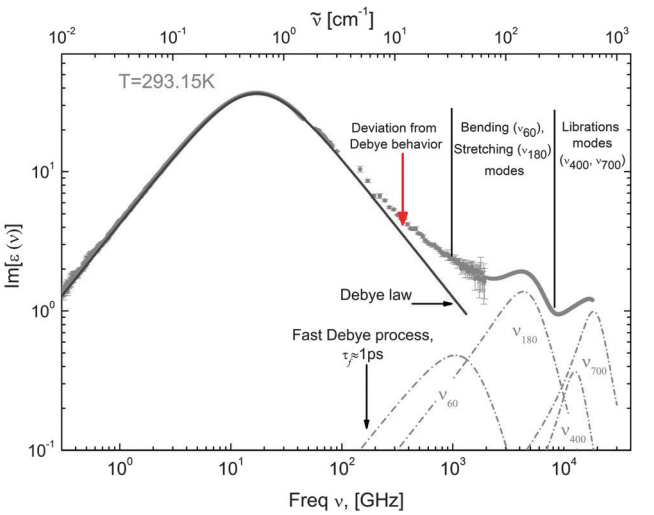

Fig. 1 The imaginary part of the complex dielectric permittivity at 20 ± 1 °C. The dielectric data were combined from different sources: for region 0.1–20 GHz, from ref. 29 and 30 at 20 °C; for region 20–100 GHz, from ref. 30 at 20 °C; for region 100 GHz–2 THz, from ref. 31 and 32 at 19.3 °C; and for the FIR region 2–18 THz, from ref. 21 at 20.2 °C. Apart from the FIR region, the error bars are given. The red arrow indicates the deviation from Debye behavior, depicted by a solid black line. The position of the fast Debye process is marked by a black arrow (the process is not shown in the figure).

with a relaxation time $\tau_D \approx 9.3$ ps at room temperature,[16] which reflects the cooperative reorientation dynamics of water.[17–20] The high frequency part of this relaxation peak is perturbed by four damped harmonic oscillators at ~60, 180, 400 and 700 cm^{-1}, which are clearly detected by both FIR[21,22] and low-frequency Raman spectroscopy[23–27] (we discuss the nature of these modes later). However, accounting for the four oscillators and one

[a] *The Hebrew University of Jerusalem, Department of Applied Physics, Edmond J. Safra Campus, Givat Ram, Jerusalem 91904, Israel. E-mail: yurif@mail.huji.ac.il*
[b] *Kazan Federal University, Institute of Physics, 420008, Kremlevskaya str.18, Kazan, Tatarstan, Russia*

Debye term is not enough to describe the total dielectric spectra with good accuracy. Therefore, an additional Debye process has been introduced[28] in order to formally fit the non-Debye behavior in the frequency range at around 0.1–1 THz. This process has been called a fast Debye process; the fitting procedure yields a relaxation time of around $\tau_f \approx 1$ ps at room temperature.[28]

Although it was noted more than 40 years ago, the physical nature of the fast Debye process is still poorly understood.[33] Two possible scenarios exist to explain this process. The first is referred to as a "*structural*" scenario and is based on the two-fraction model[28,34,35] of water, where the water is represented as a mixture of two fractions: a small fraction with either weakly H-bounded molecules or not H-bonded at all, and the other fraction with molecules essentially strongly coupled by H-bonds. Here, the fast mode was attributed to the rotations of water molecules of this weakly bonded fraction,[28] or to the non-elastic collisions of the non H-bonded water molecules.[34] This model is supported by two obvious experimental facts:

(a) The relaxation time τ_f is small and approximately equal to the collision time between water molecules in the gaseous state (with the same density as bulk water);[36]

(b) The ratio of the amplitudes of the main and fast modes coincide approximately with the fraction of molecules that form no more than two hydrogen bonds.[37]

This qualitative explanation is quite rational, but suffers from certain shortcomings. For instance, the coordination analysis performed in ref. 37, infrared spectroscopy data[38] and Raman spectroscopy results[39,40] all reveal a smooth fraction distribution ranging from undercoordinated molecules with two H-bonds to overcoordinated ones with five H-bonds. Consequently, the strong division of the water substance into just two separate fractions is questionable.

Recently the "structural" scenario has been challenged by a "*dynamic*" scenario.[41] Generally speaking, in the "dynamic" scenario, one implies that the non-Debye behavior in the THz region is caused by different molecular motions. This idea is reinforced by results obtained in ref. 24, where Dielectric and Raman spectra of water were compared. The authors of this work revealed that the relaxation peak in Raman water spectra is located in the same frequency region where non-Debye behavior manifests in the Dielectric spectra. However, the main peak of the dielectric spectra is not visible in the Raman spectra. Similar behavior was also observed for other H-bonded-liquids such as monohydric alcohols. Note that for non H-bonded liquids, this specific behavior was not observed.[24] Since Raman active components are attributed to different types of vibrations (intra- or inter-molecular), we may assume that some oscillations of the H-bond network serve as additional molecular movements in the "dynamic" scenario.

In this work, we will develop the concept of the "dynamic" scenario in liquid water. Namely, we present the model that allows the linking the Raman spectroscopy results to the non-Debye relaxation behavior in the sub-THz and THz regions. In the following sections we will start with a brief discussion about the mechanisms of dielectric relaxation in water and then consider what the marriage of Raman spectroscopy data to the dielectric spectrum data can contribute to our understanding of water relaxation. We will expand the idea of a "dynamic" scenario into a mathematical description to derive an equation for the complex dielectric permittivity, which allows fitting the dielectric spectra of water without involving the fast Debye-process.

Mechanisms of the dielectric relaxation in water

One of the first model of the dielectric relaxation of water was Debye's theory,[42] where the rotation diffusion of spherical polar molecules in a viscous continuum is considered as the main mechanism of the relaxation. However, although this model yields the correct value for the dielectric time relaxation $\tau_D = 4\pi a^3\eta/k_BT$ (where a is the radius of the sphere, and η is the viscosity), by definition it cannot be applied to the strongly associated liquids.[43,44] In particular, the rotation of the water molecule occurs within an open H-bond network rather than in a viscous continuum. Therefore, today, water's dipole rotation dynamics are assumed to be the switching between different dipole directions, rather than its continuous diffusion. Among the different bulk water relaxation models[28,34,35,41,45] the application of a wait-and-switch relaxation model to water[17,18,43,46] has recently been gaining popularity. According to this model, the reorientation of a water molecule occurs on the large angle and only when it encounters an appropriate defect of the H-bond network, otherwise the water molecule remains in a waiting mode. This waiting regime leads to a delay in the relaxation compared with the gaseous state, where the relaxation time is around 1 ps.[36] In other words, the change of the total polarization is caused by the migration of the defects through the H-bond network. However, there are still disputable issues related to the origin of these defects. Currently, the variety of defects that are proposed in the literature can be classified into two main groups: orientation (or structural) and ionic defects.

Orientation defects

The hydrogen bond between water molecules leads to localized tetrahedral ordering that restricts molecular reorientation (see Fig. 2a), in accordance with Bernal–Fowler–Pauling rules.[47,48] However, due to thermal fluctuation some molecules distort this localized structure, breaking some of the H-bonds and creating bifurcated (see Fig. 2b and c), trifurcated H-bonds, or other more complicated configurations.[49] Hereinafter we define these irregularities of the tetrahedral ordering as orientation defects. The presence of any defect in the vicinity of the water molecule facilitates its reorientation. Indeed, for example, the bifurcated hydrogen bond lowers the potential energy barrier for reorientation of the fivefold H-bonded water molecule (Fig. 2b). Hence, the fifth neighbor supports reorientation motion by the simultaneous action of two favorable effects: weakening of existing hydrogen bonds and provision of an appropriate site for the formation of a new hydrogen bond. Further migration of the orientation defects leads to consecutive reorientation of the

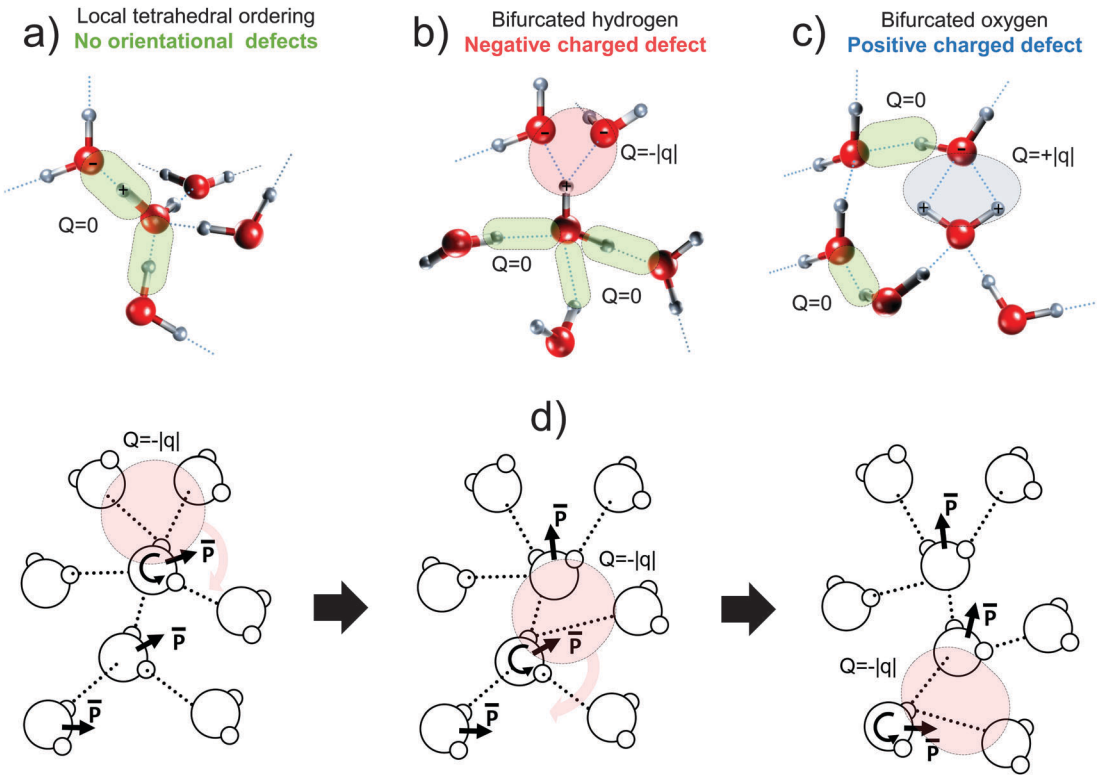

Fig. 2 Orientation defects (a) local tetrahedral ordering of the water molecules without defects. (b) The defect of the H-bond network due to bifurcated hydrogen. The negative charge, $Q = -|q|$, can be associated with this defect type (pink shaded area) regarding normal H-bond (green shaded area). (c) The defect of the H-bond network due to bifurcated oxygen. The positive charge, $Q = +|q|$, can be associated with this defect type (blue shaded area) regarding normal H-bond (green shaded area). (d) Schematic representation of the migration of orientation defects (pink shaded area) with consecutive changing of the dipole moment's direction of water molecules.

dipole moment's direction of water molecules (see Fig. 2d). Furthermore, by implying the switching reorientation of water molecules, we may then suggest the hopping of orientation defects between molecules rather than their continuous diffusion. This mechanism is described in detail in ref. 39, 40, 43, 49 and 50 and is supported by various experimental observations.[17,18,39] In a way, the orientation defects in water resemble the L–D Bjerrum defects in ice,[51] however the defects in water are smeared out and not localized as they are in ice.[49] Note that the defects in water are created as a coupled pair defect/anti-defect and are annihilated when they meet.

Ionic defects

In addition to the orientation defects, the polarization of water may be caused by the migration of H_3O^+ and OH^- pairs, also known as ionic defects[52] (see Fig. 3a). In this case, a molecule does not rotate as a whole, as it does in the orientation defect mechanism. Simply speaking, the change of the dipole direction

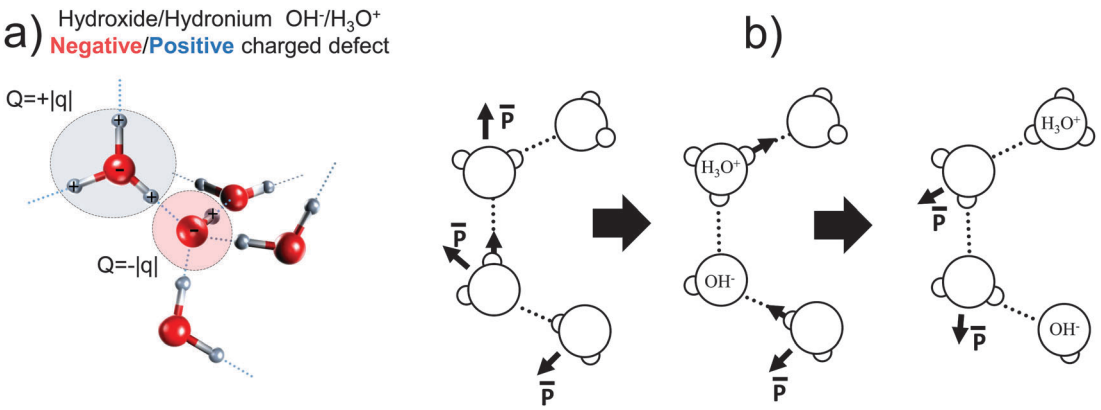

Fig. 3 Ionic defects (a) the hydroxide and hydronium defects can be associated with positive and negative charge carriers, respectively; (b) schematic representation of the generation and migration of ionic defects with the changing of the dipole moment's direction of water molecules.

of the water molecule is driven by a rearrangement of the proton position due to proton hopping:[53,54] On one side, a proton has been gained, and on the other side, a proton has been lost (see Fig. 3b). While this idea is relatively new, a similar scenario was hinted at in[55] on the origin of auto-ionization in water. Naturally, when the pairs of defects H_3O^+/OH^- meet they are annihilated just like in the case of orientation defects.

In general, the orientation and ionic defects coexist and dielectric relaxation in water should be driven by both mechanisms. However, one mechanism may play a more dominant role over the other. Moreover, one may assume a dynamic crossover between these two mechanisms. The latter can happen, for example, due to a significant difference between corresponding activation energies, as observed in bulk ice.[56] In liquid water the activation energy of ionic defect transport is around $E_A \approx 20$ kJ mol^{-1}.[53] For the transport of orientation defects in liquid water the simulation studies give approximately the same energy value.[49] The activation energy of the orientation defects for both ice and liquid water can be found experimentally by measuring the self-diffusion coefficient of the tracer molecule $H^{18}O_2$. According to Haas' idea,[57] self-diffusion takes place *via* interstitials in the H-bond network that are associated with orientation defects. Thus the migration rates of the tracers and the relaxation caused by orientation defects should be proportional, or the activation energies should coincide. Over the temperature range studied, the self-diffusion coefficient fits the standard Arrhenius expression, $D_{self} = D_0 \exp(-E_A/RT)$, where for ice E_A = 52.1–65.6 kJ mol^{-1} [58] and for water E_A = 18.4–20.1 kJ mol^{-1}.[59–61] We see that because the activation energies of the ionic and orientation defects in liquid water are equal, we cannot distinguish between them based on the dielectric spectra only. For this reason we also don't observe a dynamic crossover in dielectric time relaxation, in contrast to ice.[56] Consequently, we cannot conclude what mechanism is dominant for the main dielectric relaxation process in water from the dielectric spectra.

However, it is worth noting the strong temperature correlation of the dielectric time relaxation, τ_D, with viscosity, η ($\tau_D T/\eta$ = const),[62] and proton spin–lattice relaxation time, T_1 ($T_1\tau_D$ = const).[63,64] Furthermore, the dielectric relaxation practically does not react upon changes in pH.[65–68] Based on these experimental findings, the orientation defects in some papers[50,60,69–71] are considered to be the dominant mechanism in the dielectric relaxation. Therefore, for the remainder of this paper we will concede to the opinion presented in literature and consider only orientation defects. Nevertheless, attempts are being made to assign a leading role to the ionic defects.[52] However, this idea is supported as yet by simulation only, and we must admit that no direct experimental evidences of this exists to date.

Raman spectroscopy results: What do we know about fluctuation of the H-bond network of water?

In the case of water in the liquid state, the results of low frequency Raman spectroscopy can help us to understand the origin of the non-Debye behavior in the sub-THz region. The main relaxation peak of water is located within the overlap of the working frequency ranges of Dielectric and Raman spectroscopies. The most comprehensive analysis of the low frequency Raman spectra of water was presented in a set of papers by G. Walrafen *et al.*[26,27,72,73] and Y. Tominaga *et al.*[25,74–76] Usually, four damping oscillator modes and a wide background process are detected in the spectrum below ~1000 cm^{-1} (~30 THz), which are shown in Fig. 4(a) and (b). Corresponding oscillation modes have also been observed in FIR spectroscopy.[21] The two bands at ~700 cm^{-1} and ~400 cm^{-1} have an isotopic shift.

$\sim \sqrt{2}$ in heavy water (D_2O) and hence they can be assigned to librational motions.[73] No shift has been found for H_2O and D_2O at ~180 cm^{-1}, however a clear isotopic effect is observed between $H_2{}^{16}O$ and $H_2{}^{18}O$, as well as for $D_2{}^{16}O$ and $D_2{}^{18}O$. At the same time, the isotopic effects for both hydrogen and

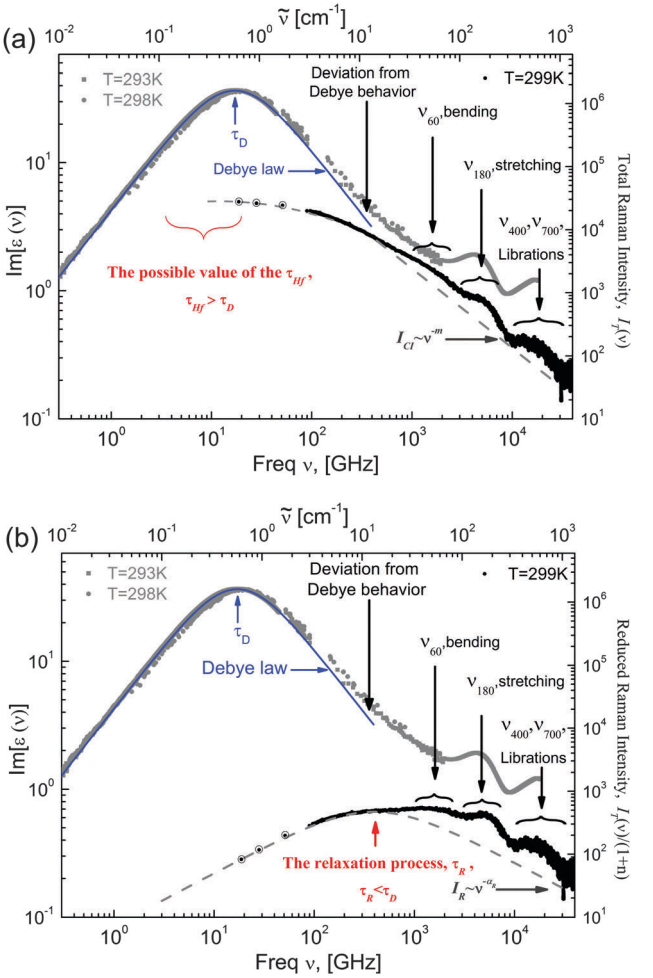

Fig. 4 Dielectric and Raman spectra. Both figures represent the dielectric spectra at 293 K, 298 K (grey squares and circles) and Raman spectra at 299 K taken from ref. 27 (black circles). The additional three points measured in Raman spectra below 3 cm^{-1} are circled. On the left panel (a) the total Raman intensity $I_T(\nu)$ is given, whereas on the right panel (b) the total intensity corrected by the Bose–Einstein correction factor $I_T(\nu)/(1 + n(\nu))$ is plotted. The dashed line in the panel (a) defines the baseline I_{Cl} which is attributed to collision-induced phenomena.[27] The dashed line in the panel (b) defines the relaxation mode, which was fitted by the Cole–Cole law.[25,76]

oxygen atoms at $\sim 60\ cm^{-1}$ are negligible.[74] This indicates that the 180 cm^{-1} mode in the Raman spectrum is caused mainly by oxygen atom vibrations, whereas the 60 cm^{-1} mode is caused by the motion of the entire water molecule.[73] Therefore, these bands have been attributed with acoustics modes usually assigned to ''H-bond stretching'' at 180 cm^{-1} and ''H-bond bending'' at 60 cm^{-1}.[77,78] Thus, as the working frequency decreases the scale of the macroscopic motions detected increases. Hence, it is logical to assume that the cooperative vibrations of several water molecules should be detected in Raman spectra at lower frequencies. However, the interpretation of the wide background mode at the extra low frequency range of the Raman spectra remains ambiguous.

G. Walrafen *et al.* were the first to measure the Raman intensity at extremely low frequencies up to 0.6 cm^{-1}.[27] The total intensity $I_T(\nu)$ measured in this work is shown in the Fig. 4a (here $I_T(\nu)$ is already corrected for λ^{-4} effect and instrumental constant). The additional three points measured below 3 cm^{-1} are circled. The wide background mode at the low frequencies extends up to the Rayleigh scattering peak. Usually, the intensity $I_T(\nu)$ obtained should be corrected by Bose–Einstein (BE) energy level population factor $1/(1 + n(\nu)) = 1 - \exp(-h\nu c/k_B T)$; the value $I_T(\nu)/(1 + n(\nu))$ is presented in Fig. 4b. However, Walrafen *et al.* claim[27] that, in water the wide background at low frequencies should be analyzed before BE factor correction. They imply that the origin of this background is related to collision-induced (CI) Raman scattering.[79] In simplified terms, the process of CI Raman scattering maybe described as follows. In Raman spectroscopy, the intensity of the scattering can be observed only, when the derivation of the polarizability with respect to the normal coordinate is not zero. As a rule, different intramolecular motions provide a change in the polarizability of water molecules and consequently the Raman active modes. However, if the molecules are engaged in collisions with one another, the electric field induced in one of the colliding molecules by the exciting radiation adds to the excited electric field at the second molecule of the collision pair. In other words, the intermolecular collisions cause the change in polarizability, inducing additional Raman modes. In the case of water and other H-bonded associated liquids, the hydrogen bonds prevent close convergence and direct collisions of water molecules. Therefore, in the case of water, CI Raman scattering can be considered as a global fluctuation of the H-bond network.[80] Thus, the fluctuation of the H-bond network leads to the change of polarizability of water molecules that activates the Raman component in the form of a wide background. This idea is also supported by the fact that this background is significantly smaller in the case of ice.[27] It is claimed in ref. 27 that these fluctuations must obey BE statistics, as required by the vibrational modes of the medium, which means that CI Raman intensity, I_{CI}, must be analyzed before BE correction (grey dashed line in Fig. 4a). The parameter I_{CI} has a power law behavior at high frequency, $I_{CI}(\nu) \sim \nu^{-m}$, indicating the existence of multiple relaxation processes of the H-bond network of water.[81] However, at low frequencies, the I_{CI} tends towards a constant regime attributed to the absence of a memory effect in the fluctuation dynamics of the H-bond network.[80] The time where this crossover occurs is considered as the characteristic time τ_{Hf} of global hydrogen-network rearrangement dynamics in liquid water.[80,81] Estimations of this time yields τ_{Hf} = 20–40 ps (see Fig. 4a). Note that simulation studies give comparable values.[80,81] This time is longer than the average lifetime of the individual hydrogen bonds, known to be about several hundred femtoseconds.[82,83] It is worth noting that the idea of the significant role of the global H-bond network dynamics in water has recently been gaining popularity.[84]

On the other hand, the BE correction factor for all Raman spectra, including CI Raman scattering,[24,25,76] is used to analyze the value $I_T(\nu)/(1 + n(\nu))$ (see Fig. 4b). In this case, the wide background of the CI process transforms into a relaxation process with time τ_R = 0.5–1.5 ps, which can be fitted *via* the Cole–Cole function[24,25,75]. The position of this relaxation process coincides approximately with the position of the assumed fast Debye process in the dielectric spectra (see Fig. 1), which supports the idea of introducing this fast process into the fitting of dielectric spectra. This relaxation time in Raman spectra has been understood as the lifetime of the localized structure (not global) between H-bonded water molecules that constitute the unit of intermolecular vibration.[74]

Thus, depending on the choice of Raman spectra analysis, there are two characteristics of H-bond network fluctuation times, τ_{Hf} and τ_R, with different physical meanings. If we accept the idea of global H-bond network fluctuations, then the time $\tau_{Hf} > \tau_D$ should be used. If we assume local fluctuations of H-bonded structures, it is appropriate to use the time $\tau_R < \tau_D$. However, in both cases it is agreed that at low frequencies, less than 50 cm^{-1} ($\approx$1.5 THz), the vibrations of the H-bond network start to play a significant role. In view of these facts, it seems that the main source of the non-Debye behavior in the THz region is H-bond vibrations. Thus, on one hand there is the defect movement through the water H-bond network, and on the other hand, this H-bond network fluctuates. In the next section, we will try to account for these vibrations theoretically to obtain an expression for the complex dielectric permittivity, which will allow us to fit the whole dielectric spectra.

The effect of H-bond network vibration on defect migration

We discussed above that the mechanism of dielectric relaxation of water, and consequently its polarization, $P(t)$, can be considered as the migration of the orientation/ionic defects through the H-bonded network. Furthermore, every defect may be associated with some effective charge carrier. In the case of the orientation defects, the locally concentrated density of hydrogen/oxygen atoms due to the rearrangements of the water molecules in the H-bond network may serve as positive or negative charge carriers (see Fig. 2d). In the case of the ionic defects, it is the pair of hydroxide and hydronium OH^-/H_3O^+ (see Fig. 3b) that serve this function. Thus, the problem of the dipole reorientation in water can be reduced to the simple problem of the migration

of the charge carriers. Based on this idea, the one-sided Fourier transform

$$f^*(\omega) = \hat{F}[f(t)] = \lim_{\delta\to 0}\int_0^\infty f(t)\mathrm{e}^{-i\omega t-\delta t}\mathrm{d}t, \quad (1)$$

of the relaxation function $\phi(t) = P(t)/P(0)$ (see Mathematical Appendix A) can be written as follows

$$\phi^*(\omega) = \frac{1}{i\omega\left[1+\dfrac{i\omega}{6k_\mathrm{B}T\varepsilon_0}\sum\limits_{i=1}^{N} n_i q_i^2\langle r_i^{*2}(\omega)\rangle\right]}. \quad (2)$$

Here q_i, n_i and $\langle r_i^{*2}(\omega)\rangle$ are the effective charge, number density and Fourier transform of the mean square displacement of the i-th type of the defect, respectively; N is the number of defect types; $\varepsilon_0 = 8.854\times10^{-12}$ F m^{-1} is the permittivity of vacuum; and k_B is the Boltzmann constant. To obtain the static dielectric permittivity $\varepsilon^*(\omega)$ we use the following relationship

$$\frac{\varepsilon^*(\omega)-\varepsilon_\infty}{\Delta\varepsilon} = \hat{F}\left[-\frac{\mathrm{d}\phi(t)}{\mathrm{d}t}\right] = 1 - i\omega\phi^*(\omega). \quad (3)$$

As a result we get

$$\varepsilon^*(\omega) = \varepsilon_\infty + \frac{\Delta\varepsilon}{1+\left[\dfrac{i\omega}{6k_\mathrm{B}T\varepsilon_0}\sum\limits_{i=1}^{n} n_i q_i^2\langle r_i^{*2}(\omega)\rangle\right]^{-1}}. \quad (4)$$

As stated above, the mechanism of the orientation defects is the most widely accepted in literature today. Furthermore, we suppose that orientation defects do not differ significantly from one another, *i.e.* we can keep only one term in the sum of eqn (4), namely $N = 1$. If necessary, the result can easily be generalized for the case of different types of defects. If the defect mobility follows normal diffusion behavior

$$\langle r^2(t)\rangle = 6D_\mathrm{defect}t, \quad (5)$$

where D_defect is the diffusion coefficient of the defect migration, then substituting the Fourier transform of eqn (5) $\langle r^{*2}(\omega)\rangle = 6D_\mathrm{defect}(i\omega)^{-2}$ into eqn (4) yields the well-recognized Debye equation

$$\varepsilon^*(\omega) = \varepsilon_\infty + \frac{\Delta\varepsilon}{1+i\omega\tau_\mathrm{defect}},\ \tau_\mathrm{defect} = \frac{k_\mathrm{B}T\varepsilon_0}{nq^2D_\mathrm{defect}}. \quad (6)$$

Note that this equation provides the perfect description of the water dielectric spectra only up to tens of GHz. Furthermore, in the previous section we concluded that the H-bond vibrations play an important role in the sub-THz range. To take this effect into account we suggest that the defect has an additional vibrational motion near the water molecule before its consequent movement. Then, the whole defect movement can be expressed as a superposition of translation $r_\mathrm{tr}(t)$ and oscillation $u_\mathrm{osc}(t)$ motions as follows

$$\langle r^2(t)\rangle = \langle (r_\mathrm{tr}(t)+u_\mathrm{osc}(t))^2\rangle = \langle r_\mathrm{tr}{}^2(t)\rangle + \langle u_\mathrm{osc}{}^2(t)\rangle, \quad (7)$$

where we assumed that translation and oscillation motions are independent. The translation term is responsible for the defect migration from one molecule to another and can still be considered to be normal diffusion $\langle r_\mathrm{tr}{}^2(t)\rangle = 6D_\mathrm{defect}t$.[85]

Obviously, the oscillation contribution reflects the vibrations of the H-bond network as a whole. Usually, the H-bond structure of water in various popular models[86–88] is considered to be a dynamic percolated H-bond network. The notation "dynamic" implies that the H-bond network continuously modifies its structural configuration through the rearrangements of the hydrogen bonds. However, at any instant of time water appears as a percolated H-bond network, which has a fractal nature.[88] To calculate the oscillations of this percolated network, the numerous hydrogens bonds between water molecules may be assigned to a great number of coupled harmonic oscillators. Furthermore, it is well-known that percolating systems are characterized by scaling behavior in the vibrational density of states $g(\omega)$, which follows the power law behavior $g(\omega)\sim\omega^{d_\mathrm{f}-1}$, where d_f is a spectral dimension.[89,90] Based on these ideas and well-known models,[91–93] we can calculate the Fourier-transform of $\langle u_\mathrm{osc}{}^2(t)\rangle$ (see Mathematical Appendix B, eqn (B9)) as follows

$$\left\langle u_\mathrm{osc}^{*2}(\omega)\right\rangle = (i\omega)^{-1}\frac{6k_\mathrm{B}Tn_\mathrm{f}}{M\omega_\mathrm{D}{}^2}\left[\frac{i\omega\gamma(\delta)}{\omega_\mathrm{D}}\right]^{-\delta},\ \delta = 2-d_\mathrm{f}, \quad (8)$$

where function $\gamma(\delta)$ is defined by eqn (B9) and is displayed in Fig. 8; the parameter M is a mass of water molecule; n_f is the number of density of vibrational modes; ω_D is the cut-off Debye frequency, which is defined by condition $g(\omega > \omega_\mathrm{D}) = 0$ (not to be confused with dielectric time relaxation, τ_D).[94] Then, for Fourier transform of total MSD (7), we get

$$\begin{aligned}\left\langle r^{*2}(\omega)\right\rangle &= \left\langle r_\mathrm{tr}^{*2}(\omega)\right\rangle + \left\langle u_\mathrm{osc}^{*2}(\omega)\right\rangle \\ &= (i\omega)^{-1}\left(6D_\mathrm{defect}(i\omega)^{-1} + \frac{6k_\mathrm{B}Tn_\mathrm{f}}{M\omega_\mathrm{D}{}^2}\left[\frac{i\omega\gamma(\delta)}{\omega_\mathrm{D}}\right]^{-\delta}\right),\end{aligned} \quad (9)$$

and substituting this equation into eqn (4), we finally obtain for the complex dielectric permittivity

$$\varepsilon^*(\omega) = \varepsilon_\infty + \frac{\Delta\varepsilon}{1+\left[(i\omega\tau_\mathrm{defect})^{-1}+(i\omega\tau_\mathrm{osc})^{-\delta}\right]^{-1}}. \quad (10)$$

where

$$\tau_\mathrm{defect} = \frac{k_\mathrm{B}T\varepsilon_0}{nq^2D_\mathrm{defect}},\ \tau_\mathrm{osc} = \frac{\gamma(\delta)}{\omega_D}\left[\frac{M\omega_\mathrm{D}{}^2\tau_\mathrm{defect}D_\mathrm{defect}}{k_\mathrm{B}Tn_\mathrm{f}}\right]^{1/\delta}. \quad (11)$$

Function (10) has the usual Debye-type behavior at low frequencies, while at high frequencies the excess wing appears with a slope equal to δ in log–log scale. The asymmetrical shapes of the spectra produced by eqn (10) at different values of δ are presented in Fig. 5.

We see that the specific behavior of function (10) behind the maximum of the losses peak allows us to describe the non-Debye behavior of the water relaxation in the sub-THz region. In this case, we have no need to introduce the additional "fast" Debye process as in the two-fraction water model. The analysis of function (10) shows that to produce an excess wing at high frequency and to keep Debye-type behavior at the low frequency part of $\varepsilon''(\omega)$, we must satisfy the condition $\tau_\mathrm{osc} > \tau_\mathrm{defect}$. This would seem counterintuitive, that a global low frequency oscillation would have a high frequency ramification, but it

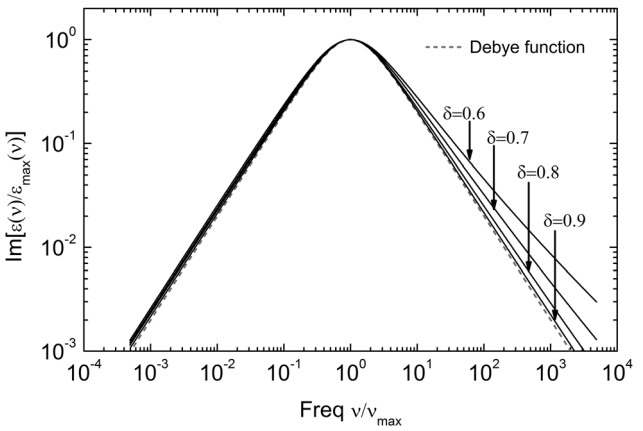

Fig. 5 Normalized model data of dielectric losses generated by eqn (10) at different values of δ. For each value of δ the spectrum is normalized by the amplitude of the main dielectric peak and the frequency scale by the characteristic of the same peak. Here we used the following parameter values: $\Delta\varepsilon$ = 75, τ_{defect} = 9 ps, τ_{osc} = 10 × τ_{defect}.

has some justification according to Walrafen *et al.*[27] for the low frequency Raman spectra, although his ideas are still hotly debated. Furthermore, our analysis showed that τ_{defect} defines the position of the main peak (the τ_{osc} corrects by just a bit the position of the main peak). Thus, in the framework of this model, we can accept the concept of the global fluctuation of the H-bond network and equate the time τ_{osc} with time τ_{Hf} from Raman scattering results (see Fig. 4a). Below, we will discuss this time in detail.

It is worth noting that equations similar to eqn (10) have been obtained in previous works from other physical principals,[56,95–98] and have been successfully applied to bulk ice Ih[56] and glass formers.[95,96] Furthermore, the high frequency limit of eqn (10) has been recognized in water/glycerol mixtures[99] and bulk water.[52]

Comparison with experiment: basic results

The fitting of the dielectric spectrum at 293 K

The ability of function (10) to shift up the high frequency wing of the loss peak allows us to describe the data presented in Fig. 1 as follows

$$\varepsilon^*(\omega) = \varepsilon_{1,\infty} + \frac{\Delta\varepsilon}{1 + \left[(i\omega\tau_{defect})^{-1} + (i\omega\tau_{osc})^{-\delta}\right]^{-1}} + \frac{A_{60}\omega_{60}{}^2}{\omega_{60}{}^2 - \omega^2 + i\omega\Gamma_{60}} + \frac{A_{180}\omega_{180}{}^2}{\omega_{180}{}^2 - \omega^2 + i\omega\Gamma_{180}} + \frac{A_{400}\omega_{400}{}^2}{\omega_{400}{}^2 - \omega^2 + i\omega\Gamma_{400}} + \frac{A_{700}\omega_{700}{}^2}{\omega_{700}{}^2 - \omega^2 + i\omega\Gamma_{700}}. \quad (12)$$

Here $\varepsilon_{1,\infty} = n^2$, where n is the refractive index; the last four terms define the damping oscillators at frequencies ~60, 180, 400 and 700 cm^{-1}, correspondingly (where $\omega_i = 2\pi\nu_i = 2\pi c\tilde{\nu}_i$, and c is the light speed). Parameters A_i and Γ_i define the amplitudes and widths of the oscillators losses. To restrict the variability in the fitting procedure we maintain ratios between absorption peaks from FIR measurements,[21] taking into account the frequency factor. Namely, we apply $A_i \sim n(\nu_i)A_i^{abs}/\nu_i$, where A_i^{abs} is the height of the absorption peak for the corresponding mode of the damped oscillator; $n(\nu_i)$ is the refractive index at the respective frequency. Furthermore, the positions of the loss peaks of the last four terms cannot significantly differ from the Raman peak positions. Since we assigned the parameter τ_{osc} to the time of global fluctuations of the H-bond network τ_{Hf} ($\tau_{osc} \approx \tau_{Hf}$), we used the boundary conditions $20 < \tau_{osc} < 40$ ps for the fitting the values, as estimated from the Raman collision-induced intensity. Following this procedure, the best fitting result is presented in Fig. 6. The fitting parameters of the first term in this case are equal to

$$\Delta\varepsilon = 7\ 5.3 \pm 1.4,\ \varepsilon_\infty = 1.7 \pm 0.3,\ \tau_{defect} = 12.4 \pm 0.2\ \text{ps},$$
$$\delta = 0.93 \pm 0.01,\ \tau_{osc} = 35 \pm 1\ \text{ps}. \quad (13)$$

The static permittivity is equal to $\varepsilon_s = \Delta\varepsilon + \varepsilon_\infty = \Delta\varepsilon + \varepsilon_{1,\infty} + A_{50} + A_{180} + A_{400} + A_{700} \approx 80$.

The position of the main relaxation peak, τ_{max}, is affected by the presence of the excess wing. From eqn (10) it is easy to show that

$$\tau_{max} \approx \tau_{defect}\cdot[1 + (\tau_{defect}/\tau_{osc})^{\delta}]^{-1} \approx 9.1\ \text{ps}, \quad (14)$$

which coincides with the value of the relaxation time, τ_D, if we use the regular Debye law for the dielectric dispersion. Here, we present data analysis for 293 K only, because the fitting procedure is very sensitive to the infrared peak position at high frequencies. Therefore, we cannot use the interpolation functions for the dielectric permittivity presented in ref. 15 and must analyze only original experimental measurements for the frequency band under consideration, currently available only for 293 K. Parameter δ is most probably related to the power law parameter, m, of the collision-induced base line from the Raman scattering results $I_{CI}(\nu) \sim \nu^{-m}$ (see Fig. 4a). The derivation of this relationship is a separate issue and is outside the scope of this paper. However, the master plot for the main peak and excess wing of the dielectric spectra up to 70 °C was revealed in the work.[52] It implies the rather slow temperature dependence of $\delta(T)$ and approximately the same temperature dependences for both τ_{defect} and τ_{osc}.

The calculation of the static dielectric permittivity of the water

As usual, the static dielectric permittivity of liquid water is calculated *via* the Kirkwood's formula, which is applicable to dipolar associated liquids in general[44]

$$\Delta\varepsilon = \varepsilon_s - \varepsilon_\infty = \frac{3\varepsilon_s}{2\varepsilon_s + \varepsilon_\infty}\left(\frac{\varepsilon_\infty + 2}{3}\right)^2 \frac{N_0\mu_d{}^2}{3k_B T\varepsilon_0}(1 + z\overline{\cos\theta}), \quad (15)$$

where μ_d = 1.84 ± 0.02 D is the dipole moment of the single water molecule in the gas phase;[2–5] $N_0 = \rho N_A/M_{H_2O}$ is the concentration of the water molecules, ρ is the density of water, M_{H_2O} is the molar mass, N_A is Avogadro's number; $\overline{\cos\theta} = 1/3$[44] is an average cosine value of angle θ between neighboring dipoles; z is the number of closest neighbors. At the classical

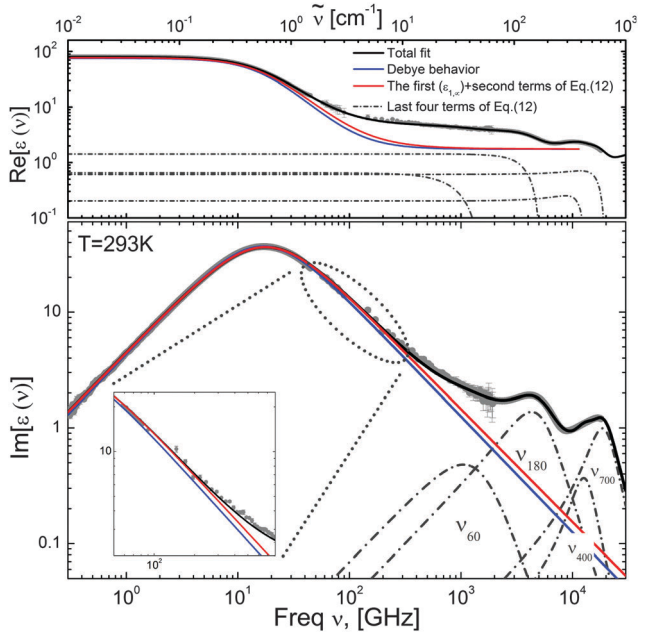

Fig. 6 Fitting of the dielectric spectrum of water at 20 °C presented Fig. 1. The black curve is the fitting curve according to eqn (12). The red curve represents the sum of the first ($\varepsilon_{1,\infty}$) and second terms of eqn (12). The grey dashed curves describe the four last terms of eqn (12). The blue curve represents Debye-type behavior.

value $z = 4$ we have $\Delta\varepsilon \approx 62$ at $T = 293$ K, which does not satisfy the experimental results. However, on the other hand, in the framework of the present model, it is easy to find the relationship between dielectric strength $\Delta\varepsilon = \varepsilon_s - \varepsilon_\infty$ and parameters of the defect migration. The dielectric strength may be written as follows (see Mathematical Appendix A, eqn (A13)–(A16))

$$\Delta\varepsilon = \varepsilon_s - \varepsilon_\infty = \frac{nq^2}{6k_B T\varepsilon_0}R^2,\ R^2 = \lim_{t\to\infty}\langle r^2(t)\rangle, \qquad (16)$$

where R^2 is the maximum value of the MSD of the defect. The limited value for MSD indicates that defects have a finite mean lifetime $\tau_{life} = \tau_{hop}R/\lambda_{hop}$, where τ_{hop} and λ_{hop} are the mean time and length of one defect hop. The lifetime of a defect is defined by the time interval from the defect birth to its annihilation with an anti-defect (see above). Therefore, we can define the parameter R as a correlation length between water molecules that can also be associated with a minimal water cluster size. Then, we can define the number of closest neighbors as $z = R/\lambda_{hop}$. Using the expression for the time relaxation τ_{defect} (11), we can write

$$R^2 = \frac{6\Delta\varepsilon k_B T\varepsilon_0}{nq^2} = 6\Delta\varepsilon D_{defect}\tau_{defect},$$
$$z = \frac{1}{\lambda_{hop}}\sqrt{6\Delta\varepsilon D_{defect}\tau_{defect}}. \qquad (17)$$

Thus, from the eqn (17) it follows that parameter z depends on $\Delta\varepsilon$. Taking this into account and solving the system of eqn (15) and (17), we obtain the more accurate temperature dependence for $\Delta\varepsilon(T)$, presented in Fig. 7a. In this case we obtain the more appropriate value of $\Delta\varepsilon \approx 74$ at $T = 293$ K.

Here, we assume that the defect diffusion and the self-diffusion of the water molecules are the same, *i.e.* $D_{defect} \approx D_{self}$, and use the experimental fact that the multiplication of the self-diffusion coefficient and the dielectric time relaxation practically do not depend on the temperature $\tau_{defect}D_{self} \approx \tau_D D_{self}$ = const = $(1.8 \pm 0.2) \times 10^{-20}$ m^2.[62] The parameter λ_{hop} was chosen as $\lambda_{hop} \approx 2\lambda_{O\text{–}O}$, where $\lambda_{O\text{–}O} \approx 2.7$ Å is the distance between oxygen atoms (see Fig. 2d).

Using eqn (17) we may calculate the temperature dependence of the number of closest neighbors $z(T)$ that is presented in Fig. 7b. Here we can see that $z \approx 5.2$ at $T = 293$ K, as confirmed by X-ray and neutron scattering results.[100]

The influence of defect migration and global fluctuation of the H-bond network on dielectric and Raman spectra

In the proposed model, we have introduced two channels of energy absorption. One is attributed to the energy dissipation due to the defect diffusion with relaxation time $\tau_{defect} \approx \tau_D$, and the other is related to the global fluctuations of the H-bond network with relaxation time $\tau_{Hf} \approx \tau_{osc}$. These fluctuations change the polarizability of water molecules and absorbs the energy of the external electromagnetic field. The process with time $\tau_{Hf} \approx \tau_{osc}$ is revealed in Raman spectroscopy in the form

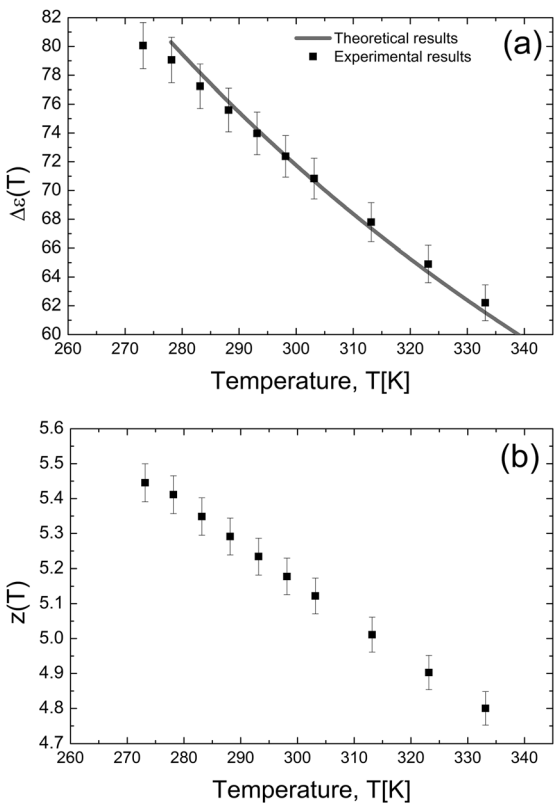

Fig. 7 (a) The temperature dependence $\Delta\varepsilon(T)$ is found from the solution of the system eqn (15) and (17) (grey line) and experimental values are taken from ref. 15. (b) The temperature dependence of the number of the closest neighbors in water $z(T)$ is calculated using eqn (17).

of a wide collision-induced background (Fig. 4a). The process with the time $\tau_{defect} \approx \tau_D$ is not Raman active because the significant change of molecular polarizability does not occur at defect migration. Indeed, we came to the conclusion that orientation defects play a dominant role in the relaxation process in comparison with proton hopping. The former implies the rotation of the molecule as a whole, without significant deformation of its electronic clouds. We stress here that Raman spectroscopy measures scattering processes but not absorption ones. On the other hand, in dielectric relaxation both of the energy absorption channels should take place: defect migration and H-bond fluctuations. However, these channels are parallel and relaxation of water occurs *via* the faster channel with the shorter relaxation time, namely *via* defect diffusion with time $\tau_{defect} \approx \tau_D$, which defines the main relaxation peak. Therefore, an additional process with time $\tau_{Hf} \approx \tau_{osc}$ is not observed in the dielectric spectra. The H-bond fluctuations appear in dielectric spectra only at high frequencies, when the defect movement becomes negligible (its free path tends to zero). Since the fluctuations obey the power law behavior (B8) they lead to the appearance of the excess wing and non-Debye behavior at sub-THz region. In mathematical terms, we can explain the scenario as follows. The normal law for diffusion (5) leads to the Debye-type behavior, however, accounting for the H-bond network vibrations leads to the appearance of an anomalous diffusion correction (7) and (B8). In turn, the anomalous behavior is significant at the short time scale or at the high frequency range, which explains the non-Debye behavior.

Conclusion

The complete dielectric spectra of water in the wide frequency range (up to 10 THz) was described by the model using only two mechanisms: defect migration and global fluctuations of the H-bond network. In the framework of this model, we describe the non-Debye behavior of the dielectric loss peak of water in the sub-THz region without involving the secondary fast Debye process. We found that the origin of this deviation from the Debye-law is an additional energy absorption due to the H-bond network vibrations. In turn, the main Debye-like peak is attributed to the defect migration. Besides the dynamical properties, we found the relationship between the static dielectric permittivity and the correlation length between water molecules. It was shown that this length is limited to the defect lifetime and can be associated with the minimal size of a water cluster. In turn, this correlation length allowed us to calculate the number of closest neighbors of a water molecule $z > 4$. Taking this and Kirkwood's formula into account, we derived a more accurate equation for the temperature dependence of the static dielectric permittivity, which was in good agreement with the experimental data.

In summary, we emphasize that this approach allows the reduction of the many-body interaction problem of H-bonded systems to the well-examined problem of the random walk (RWP). The RWP was studied comprehensively for one-, two- and three-dimensional systems. Consequently, this approach may be helpful in the description of water dynamics in various geometrical confinements including biological systems.

Mathematical Appendix A: the relationship between the relaxation function and mean square displacement of defects

Our model suggests that every defect can be associated with effective charge carriers. The jumping of the charge carriers from one water molecule (that acts as a dipole unit of the system) to another leads to a change in the direction of its dipole moments and, as a consequence, to a change of the total polarization of the sample. We now consider only one type of charge carriers and will generalize later for several types.

Let us consider a homogeneous, isotropic dielectric under an external static electric field, $\mathbf{E}_{ex}(\mathbf{r})$. If the dielectric remains under the influence of field, $\mathbf{E}_{ex}(\mathbf{r})$ over a long period of time, it reaches an equilibrium state with some stationary distribution of charge carriers, $\rho(\mathbf{r})$. If we switch off the external field $\mathbf{E}_{ex}(\mathbf{r})$ at $t = 0$, the distribution of charge carriers $\rho(\mathbf{r})$ becomes in itself a source of some field $\mathbf{E}_c(\mathbf{r})$, defined by equation $\nabla\cdot\mathbf{E}_c(\mathbf{r}) = \rho(\mathbf{r})/\varepsilon_0$. In turn, the field $\mathbf{E}_c(\mathbf{r})$ affects the charge carriers and changes the distribution density, $\rho(\mathbf{r})$. Therefore, we have a non equilibrium case and both $\mathbf{E}_c(\mathbf{r})$ and $\rho(\mathbf{r})$ should be defined as functions of time: $\mathbf{E}_c(\mathbf{r}) \rightarrow \mathbf{E}_c(t,\mathbf{r})$ and $\rho(\mathbf{r}) \rightarrow \rho(t,\mathbf{r})$. Then, assuming there are no external charges ($\rho_{ext} = 0$), *i.e.*, the total charge of the medium is zero, we can write

$$\nabla\cdot\mathbf{E}_c(t,\mathbf{r}) = \rho(t,\mathbf{r})/\varepsilon_0, \tag{A1}$$

where $\varepsilon_0 = 8.854 \times 10^{-12}$ F m^{-1} is the permittivity of vacuum. In turn, from the linear response theory, the polarization $P(t,\mathbf{r})$ at time t and at point $\mathbf{r}$ can be written as

$$\begin{aligned}\mathbf{P}(t,\mathbf{r}) &= \mathbf{P}(0,\mathbf{r}) - \varepsilon_0\chi\int_0^t \mathrm{d}t'\int_{\Delta V}\mathrm{d}V' f_p(\mathbf{r}-\mathbf{r}',\ t-t')\mathbf{E}_c(t',\mathbf{r}') \\ &= \mathbf{P}(0,\mathbf{r}) - \varepsilon_0\chi\int_0^t \mathrm{d}t' f_p(t-t')\mathbf{E}_c(t',\mathbf{r}),\end{aligned} \tag{A2}$$

where $P(0,\mathbf{r})$ is the initial polarization. Here, we have neglected spatial dispersion and imply a localized response of the material, *i.e.*, $f_p(t,\mathbf{r}) = f_p(t)\delta(\mathbf{r})$, where $f_p(t)$ is a pulse-response function of the polarization.[101] In the absence of external charges, $\rho_{ext} = 0$. Thus, for the total polarization we can write

$$\nabla\cdot\mathbf{P}(t,\mathbf{r}) = -\rho(t,\mathbf{r}). \tag{A3}$$

The created field, $\mathbf{E}_c(t,\mathbf{r})$, in turn induces a current of charge carriers. As noted above, the translation motion of the charge carriers is accompanied by the rotation of the molecular dipoles, *i.e.* changing the $\mathbf{P}(t,\mathbf{r})$. Thus, the induced current

can be defined as the time derivative of the total polarization $\mathbf{j} = \partial\mathbf{P}(t,\mathbf{r})/\partial t$. From eqn (A2), we have

$$\mathbf{j}(t,\mathbf{r}) = -\varepsilon_0\chi f_p(0)\mathbf{E}_c(t,\mathbf{r}) + \int_0^t \sigma_c(t-t')\mathbf{E}_c(t',\mathbf{r})\mathrm{d}t', \qquad (A4)$$

where we denote $\sigma_c(t) = -\varepsilon_0\chi\partial f_p(t)/\partial t$. A Fourier-transformed $\sigma_c(t)$ defines the frequency-dependent complex conductivity, $\sigma_c^*(\omega)$. Note, that here the conductivity defines only the defects transfer. Furthermore, the initial condition $\mathbf{j}(0,\mathbf{r}) = 0$ leads to $f_p(0) = 0$.

The conservation of the charge carriers is expressed by the continuity equation $\partial\rho(t,\mathbf{r})/\partial t + \nabla\cdot j(t,\mathbf{r}) = 0$. Substituting $\mathbf{j}(t,\mathbf{r})$ from eqn (A4) (with the condition $f_p(0) = 0$), and then taking under the time integration and using eqn (A1), we have

$$\frac{\partial}{\partial t}\rho(t,\mathbf{r}) + \frac{1}{\varepsilon_0}\int_0^t \sigma_c(t-t')\rho(t',\mathbf{r})\mathrm{d}t' = 0. \qquad (A5)$$

By one-sided Fourier transform of eqn (A5) we find that

$$i\omega\cdot\rho^*(\omega,\mathbf{r}) - \rho(0,\mathbf{r}) + \frac{1}{\varepsilon_0}\sigma_c^*(\omega)\rho^*(\omega,\mathbf{r}) = 0, \qquad (A6)$$

where $\rho(0,\mathbf{r})$ is the density of the charges at time $t = 0$. From eqn (A6) we find that

$$\rho^*(\omega,\mathbf{r}) = \frac{\rho(0,\mathbf{r})}{i\omega + \sigma_c^*(\omega)/\varepsilon_0} = \rho(0,\mathbf{r})\gamma^*(\omega),$$
$$\gamma^*(\omega) = \frac{1}{i\omega + \sigma_c^*(\omega)/\varepsilon_0}. \qquad (A7)$$

Thus, $\rho^*(\omega,\mathbf{r})$ is a separate function of the variables $\mathbf{r}$ and ω. In turn, from eqn (A3) we find that function $\mathbf{P}(t,\mathbf{r})$ is also a separate function, $P(t,\mathbf{r}) = \mathbf{P}_r(\mathbf{r})P(t)$. We can thus conclude that

$$\frac{\rho(t,\mathbf{r})}{\rho(0,\mathbf{r})} = \frac{\nabla\cdot\mathbf{P}(t,\mathbf{r})}{\nabla\cdot\mathbf{P}(0,\mathbf{r})} = \frac{P(t)\nabla\cdot\mathbf{P}_r(\mathbf{r})}{P(0)\nabla\cdot\mathbf{P}_r(\mathbf{r})} = \phi(t). \qquad (A8)$$

From eqn (A7) and (A8) it follows that the relaxation function

$$\phi^*(\omega) = \frac{1}{i\omega + \sigma_c^*(\omega)/\varepsilon_0}. \qquad (A9)$$

If we consider N types of charge carriers we can rewrite eqn (A9) as

$$\phi^*(\omega) = \frac{1}{i\omega + \sum_{i=1}^{N}\sigma_c^{*i}(\omega)/\varepsilon_0}, \qquad (A10)$$

where $\sigma_c^{*i}(\omega)$ denotes i-types of charge carriers. It is assumed that different types of carriers are not correlated to each other. It is worth noting that the defined conductivity $\sigma_c^*(\omega)$ is not the total macroscopic ac conductivity $\sigma^*(\omega)$ that is related to the complex dielectric permittivity *via* $\sigma^*(\omega) = i\omega\varepsilon_0\varepsilon^*(\omega)$. The relationship between them can be found in ref. 102.

Using the relationship between the frequency-dependent conductivity and the Fourier transform of the mean-squared displacement (MSD) $\langle r^2(t)\rangle$[103]

$$\sigma^*(\omega) = -\omega^2\frac{nq^2}{6k_BT}\lim_{\delta\to 0}\int_0^\infty \langle r^2(t)\rangle \exp(-i\omega t - \delta t)\mathrm{d}t, \qquad (A11)$$

where n is the number density of the mobile carriers, q is the carrier charge, and k_B is the Boltzmann constant, we finally obtain from (A10) that

$$\phi^*(\omega) = \frac{1}{i\omega\left[1 + \frac{i\omega}{6k_BT\varepsilon_0}\sum_{i=1}^{N} n_i q_i^2\langle r_i^{*2}(\omega)\rangle\right]}, \qquad (A12)$$

where $\langle r^{*2}(\omega)\rangle$ defines the Fourier transform of the MSD $\langle r^2(t)\rangle$.

Static permittivity

To find the static case instead of the relaxation eqn (A2) (at shutdown of the external field) we must consider the evaluation equation at the switch on of the external field. In this case, eqn (A2) transforms into

$$\mathbf{P}(t,\mathbf{r}) = \varepsilon_0\chi\int_0^t \mathrm{d}t' f_p(t-t')\mathbf{E}_{ex}(t',\mathbf{r}). \qquad (A13)$$

Now, however, that the step function $f_p(t)$ is an increasing function, therefore we must define the conductivity as $\sigma_c(t) = \varepsilon_0\chi\partial f_p(t)/\partial t$. Then, in the case of constant field $\mathbf{E}_{ex}(t,\mathbf{r}) = E\cdot\mathbf{e}_z$, where E = const, we have

$$P(t) = |\mathbf{P}(t)| = E\int_0^t (t-t')\sigma(t')\mathrm{d}t'. \qquad (A14)$$

Using the definition of the static dielectric permittivity[44] and the relationship (A11), we finally obtain

$$\Delta\varepsilon = \varepsilon_s - \varepsilon_\infty = \frac{P(t\to\infty)}{\varepsilon_0 E} = \frac{nq^2}{6k_BT\varepsilon_0}R^2,$$
$$R^2 = \lim_{t\to\infty}\langle r^2(t)\rangle, \qquad (A15)$$

where R^2 can be defined as a maximal MSD of the defect. In the case of N types of defect we have

$$\Delta\varepsilon = \varepsilon_s - \varepsilon_\infty = \frac{1}{6k_BT\varepsilon_0}\sum_{i=1}^{N} n_i q_i^2 R_i^2. \qquad (A16)$$

Mathematical Appendix B: the calculation of the vibration mode in a fractal H-bond network

The required expression for the oscillation part $\langle u_{osc}^2(t)\rangle$ in eqn (7) is equal by definition to

$$\langle u_{osc}^2(t)\rangle = \int_0^\infty r^2 G_s(\mathbf{r},t)\mathrm{d}\mathbf{r}, \qquad (B1)$$

where $G_s(\mathbf{r},t)$ is the self-correlation function which defines the probability of finding the atom (in our case, the water molecule) at $\mathbf{r}$ and time t that was at the origin at time 0. Assuming that the liquid water appears as a network of coupled harmonic oscillators with vibrational density of states $g(\omega)$, we can use the well-known results of van Hove[92] and Vineyard[93] for the isotropic case[91] to calculate $G_s(\mathbf{r},t)$

$$G_s(\mathbf{r},t) = [\pi w^2(t)]^{-3/2}\exp[-r^2/w^2(t)], \qquad (B2)$$

where

$$w^2(t) = 4(L(0) - L(t)),$$
$$L(t) = \frac{\hbar}{2MN}\int \frac{g(\omega)}{\omega}\left[1 - \exp\left(-\frac{\hbar\omega}{k_B T}\right)\right]^{-1} \times \left[\exp(i\omega t). + \exp\left(-it\omega - \frac{\hbar\omega}{k_B T}\right)\right]d\omega. \quad (B3)$$

Here M is the mass of the water molecule; N is the concentration of water molecules. In the liquid case, the many-phonon processes become significant that corresponds to the high temperature limit. In this case ($k_B T \gg \hbar\omega$)

$$w^2(t) = \frac{4k_B T}{MN}\int \frac{g(\omega)}{\omega^2}(1 - \cos\omega t)d\omega. \quad (B4)$$

The result strongly depends on the choice of the state density function $g(\omega)$. In the case of the simple Debye spectrum $g(\omega) = 3N\omega^2/{\omega_D}^3$, where ω_D is the Debye frequency ($g(\omega > \omega_D) = 0$), we obtain the classical result[93]

$$\langle {u_{osc}}^2(t)\rangle = \frac{3}{2}w^2(t) = \frac{18k_B T}{M{\omega_D}^2}\left[1 - \frac{\sin\omega_D t}{\omega_D t}\right]. \quad (B5)$$

However, the expression (B5) is valid only for the solid state, when we have an ideal 3D lattice with intact oscillators. If we consider water as a H-bond network with a fractal spectral dimension equals to d_f, the density state $g(\omega)$ for acoustic modes ($\omega \sim k$) is specified as[89,90]

$$g(\omega) = d_f N_f \frac{\omega^{d_f - 1}}{\omega_D^{d_f}},\ d_f = \frac{2D_H}{2 + \theta}. \quad (B6)$$

Here parameter θ is related to the diffusion type of defect through the H-bond network;[104] D_H is the Hausdorff dimension; the parameter N_f defines the total number of normal modes of vibration. Thus, substituting eqn (B6) into eqn (B4), we obtain

$$\langle {u_{osc}}^2(t)\rangle = \frac{3}{2}w^2(t) = \frac{6k_B T d_f n_f}{M\omega_D^{d_f}} t^{(2-d_f)}\int_0^{\omega_D t} x^{d_f - 3}(1 - \cos x)dx. \quad (B7)$$

where $n_f = N_f/N$ is the concentration of normal vibration modes. Working in the frequency range up to 1 THz we can set $t \gg {\omega_D}^{-1}$. Moreover, the integrants in (B7) decay as a power law (at $d_f < 3$), therefore we can extend the upper limit in the integrals into infinity. As result we have

$$\langle {u_{osc}}^2(t)\rangle = \frac{6k_B T n_f(2 - \delta)}{M{\omega_D}^{2-\delta}}\cos\left(\frac{\pi\delta}{2}\right)\frac{\Gamma(1 - \delta)}{\delta}t^{\delta},\quad \delta = 2 - d_f. \quad (B8)$$

Thus, the influence of the H-network vibrations on the defect migration leads to its anomalous diffusion. The one-sided Fourier transform of eqn (B8) is

$$\langle u^{*2}_{osc}(\omega)\rangle = (i\omega)^{-1}\frac{6k_B T n_f}{M{\omega_D}^2}\left[\frac{i\omega\gamma(\delta)}{\omega_D}\right]^{-\delta},\ \gamma(\delta) = \left[\frac{\pi(2 - \delta)}{2\sin(\pi\delta/2)}\right]^{-1/\delta}. \quad (B9)$$

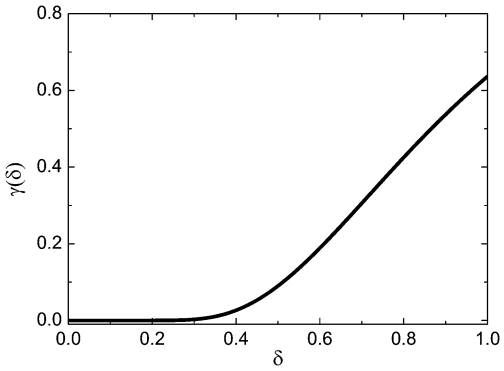

Fig. 8 The dependence of the function $\gamma(\delta)$ (B9) on δ.

The function $\gamma(\delta)$ is displayed in Fig. 8.

Acknowledgements

The authors are grateful to Prof. V. Ilyin for valuable discussions. The work was supported by the Valazzi-Pikovsky Fellowship (Lady Davis Fellowship). The work was supported in part by the Russian Government Program of Competitive Growth of the Kazan Federal University. IP and AKh acknowledge support in part by the Russian Ministry of Education and Science.

References

1 P. Ball, *Nature*, 2008, **452**, 291–292.
2 J. B. Hasted, *Aqueous dielectrics*, Chapman and Hall Distributed in the U.S.A. by Halsted Press, a division of J. Wiley & Sons, New York, London, 1973.
3 D. A. Kemp and M. S. Gordon, *J. Phys. Chem. A*, 2008, **112**, 4885–4894.
4 S. L. Shostak, W. L. Ebenstein and J. S. Muenter, *J. Chem. Phys.*, 1991, **94**, 5875–5882.
5 S. L. Shostak and J. S. Muenter, *J. Chem. Phys.*, 1991, **94**, 5883–5890.
6 Y. Marechal, *The hydrogen bond and the water molecule: the physics and chemistry of water, aqueous and bio media*, Elsevier, Amsterdam, Boston, 1st edn, 2007.
7 B. Guillot, *J. Mol. Liq.*, 2002, **101**, 219–260.
8 J. L. F. Abascal and C. Vega, *J. Chem. Phys.*, 2005, **123**, 234505.
9 H. J. C. Berendsen, J. R. Grigera and T. P. Straatsma, *J. Phys. Chem.*, 1987, **91**, 6269–6271.
10 S. Izadi, R. Anandakrishnan and A. V. Onufriev, *J. Phys. Chem. Lett.*, 2014, **5**, 3863–3871.
11 W. L. Jorgensen, J. Chandrasekhar, J. D. Madura, R. W. Impey and M. L. Klein, *J. Chem. Phys.*, 1983, **79**, 926–935.
12 G. Lamoureux, A. D. MacKerell and B. Roux, *J. Chem. Phys.*, 2003, **119**, 5185–5197.

13 M. W. Mahoney and W. L. Jorgensen, *J. Chem. Phys.*, 2000, **112**, 8910–8922.
14 M. Sega and C. Schroder, *J. Phys. Chem. A*, 2015, **119**, 1539–1547.
15 W. J. Ellison, *J. Phys. Chem. Ref. Data*, 2007, **36**, 1–18.
16 U. Kaatze, *Meas. Sci. Technol.*, 2007, **18**, 967–976.
17 F. Sciortino, A. Geiger and H. E. Stanley, *J. Chem. Phys.*, 1992, **96**, 3857–3865.
18 F. Sciortino, A. Geiger and H. E. Stanley, *Nature*, 1991, **354**, 218–221.
19 T. Sato and R. Buchner, *J. Chem. Phys.*, 2003, **119**, 10789–10800.
20 U. Kaatze, R. Behrends and R. Pottel, *J. Non-Cryst. Solids*, 2002, **305**, 19–28.
21 H. R. Zelsmann, *J. Mol. Struct.*, 1995, **350**, 95–114.
22 J. B. Hasted, S. K. Husain, F. A. M. Frescura and J. R. Birch, *Chem. Phys. Lett.*, 1985, **118**, 622–625.
23 Y. Amo and Y. Tominaga, *Phys. Rev. E: Stat. Phys., Plasmas, Fluids, Relat. Interdiscip. Top.*, 1998, **58**, 7553–7560.
24 T. Fukasawa, T. Sato, J. Watanabe, Y. Hama, W. Kunz and R. Buchner, *Phys. Rev. Lett.*, 2005, **95**, 197802.
25 Y. Tominaga, A. Fujiwara and Y. Amo, *Fluid Phase Equilib.*, 1998, **144**, 323–330.
26 G. E. Walrafen, *J. Phys. Chem.*, 1990, **94**, 2237–2239.
27 G. E. Walrafen, M. S. Hokmabadi, W. H. Yang, Y. C. Chu and B. Monosmith, *J. Phys. Chem.*, 1989, **93**, 2909–2917.
28 R. Buchner, J. Barthel and J. Stauber, *Chem. Phys. Lett.*, 1999, **306**, 57–63.
29 E. Levy, A. Puzenko, U. Kaatze, P. Ben Ishai and Y. Feldman, *J. Chem. Phys.*, 2012, **136**, 114502.
30 W. J. Ellison, K. Lamkaouchi and J. M. Moreau, *J. Mol. Liq.*, 1996, **68**, 171–279.
31 C. Ronne, L. Thrane, P. O. Astrand, A. Wallqvist, K. V. Mikkelsen and S. R. Keiding, *J. Chem. Phys.*, 1997, **107**, 5319–5331.
32 C. Mätzler and Institution of Engineering and Technology, *Thermal microwave radiation: applications for remote sensing*, Institution of Engineering and Technology, London, 2006.
33 N. V. Chekalin and M. I. Shakhparonov, *J. Struct. Chem.*, 1968, **9**, 789–790.
34 H. Yada, M. Nagai and K. Tanaka, *Chem. Phys. Lett.*, 2008, **464**, 166–170.
35 C. Ronne, P. O. Astrand and S. R. Keiding, *Phys. Rev. Lett.*, 1999, **82**, 2888–2891.
36 K. Okada, M. Yao, Y. Hiejima, H. Kohno and Y. Kajihara, *J. Chem. Phys.*, 1999, **110**, 3026–3036.
37 G. G. Malenkov, D. L. Tytik and E. A. Zheligovskaya, *J. Mol. Liq.*, 1999, **82**, 27–38.
38 J. B. Brubach, A. Mermet, A. Filabozzi, A. Gerschel and P. Roy, *J. Chem. Phys.*, 2005, **122**, 184509.
39 N. A. Chumaevskii and M. N. Rodnikova, *Dokl. Akad. Nauk*, 1999, **364**, 640–642.
40 N. A. Chumaevskii, M. N. Rodnikova and D. A. Sirotkin, *J. Mol. Liq.*, 1999, **82**, 39–46.
41 A. Y. Zasetsky, *Phys. Rev. Lett.*, 2011, **107**, 117601.
42 P. Debye, *Journal of the Society of Chemical Industry*, ed. V. Raicu and Yu. Feldman, Chemical Catalog Co., Inc., New York, 1929, vol. 48, pp. 1036–1037.
43 *Dielectric Relaxation in Biological Systems. Physical Principles, Methods, and Applications*, ed. V. Raicu and Yu. Feldman, Oxford University Press, 2015.
44 H. Frohlich, *Theory of Dielectrics. Dielectric Constant and Dielectric Loss*, Clarendon Press, Oxford, 1950.
45 A. A. Volkov, V. G. Artemov and A. V. Pronin, *Europhys. Lett.*, 2014, **106**, 46004.
46 K. S. Singwi and A. Sjolander, *Phys. Rev.*, 1960, **119**, 863–871.
47 J. D. Bernal and R. H. Fowler, *J. Chem. Phys.*, 1933, **1**, 515–548.
48 L. Pauling, *J. Am. Chem. Soc.*, 1935, **57**, 2680–2684.
49 N. Agmon, *Acc. Chem. Res.*, 2012, **45**, 63–73.
50 D. Laage and J. T. Hynes, *Science*, 2006, **311**, 832–835.
51 R. Podeszwa and V. Buch, *Phys. Rev. Lett.*, 1999, **83**, 4570–4573.
52 P. Ben Ishai, S. R. Tripathi, K. Kawase, A. Puzenko and Y. Feldman, *Phys. Chem. Chem. Phys.*, 2015, **17**, 15428–15434.
53 N. Agmon, *Chem. Phys. Lett.*, 1995, **244**, 456–462.
54 D. Marx, M. E. Tuckerman, J. Hutter and M. Parrinello, *Nature*, 1999, **397**, 601–604.
55 P. L. Geissler, C. Dellago, D. Chandler, J. Hutter and M. Parrinello, *Science*, 2001, **291**, 2121–2124.
56 I. Popov, A. Puzenko, A. Khamzin and Y. Feldman, *Phys. Chem. Chem. Phys.*, 2015, **17**, 1489–1497.
57 C. Haas, *Phys. Rev. Lett.*, 1962, **3**, 126–128.
58 P. V. Hobbs, *Ice physics*, Clarendon Press, Oxford, 1974.
59 A. J. Easteal, W. E. Price and L. A. Woolf, *J. Chem. Soc., Faraday Trans. 1*, 1989, **85**, 1091–1097.
60 D. S. Eisenberg and W. Kauzmann, *The structure and properties of water*, Clarendon Press, Oxford University Press, Oxford, New York, 2005.
61 M. Holz, S. R. Heil and A. Sacco, *Phys. Chem. Chem. Phys.*, 2000, **2**, 4740–4742.
62 J. H. Sluyters and M. Sluyters-Rehbach, *ChemPhysChem*, 2013, **14**, 3788–3800.
63 K. Krynicki, *Physica*, 1966, **32**, 167–178.
64 N. A. Melnichenko and A. S. Vyskrebentsev, *J. Struct. Chem.*, 2009, **50**, 461–469.
65 J. H. Christensen, A. J. Smith, R. B. Reed and K. L. Elmore, *J. Chem. Eng. Data*, 1966, **11**, 60–63.
66 A. S. Lileev, D. V. Loginova and A. K. Lyashchenko, *Mendeleev Commun.*, 2007, **17**, 364–365.
67 A. K. Lyashchenko, V. S. Goncharov and P. S. Yastremskii, *J. Struct. Chem.*, 1976, **17**, 396–399.
68 W. C. Qiao, K. J. Yang, A. Thoma and T. Dekorsy, *J. Infrared, Millimeter, Terahertz Waves*, 2012, **33**, 1029–1038.
69 A. Geiger, M. Kleene, D. Paschek and A. Rehtanz, *J. Mol. Liq.*, 2003, **106**, 131–146.
70 D. Laage, G. Stirnemann, F. Sterpone and J. T. Hynes, *Acc. Chem. Res.*, 2012, **45**, 53–62.
71 R. Ludwig, *ChemPhysChem*, 2007, **8**, 44–46.
72 G. E. Walrafen, *J. Chem. Phys.*, 1964, **40**, 3249–3256.
73 G. E. Walrafen, *J. Chem. Phys.*, 1966, **44**, 1546–1558.
74 Y. Amo and Y. Tominaga, *Physica A*, 2000, **276**, 401–412.

75 K. Mizoguchi, Y. Hori and Y. Tominaga, *J. Chem. Phys.*, 1992, **97**, 1961–1968.
76 K. Mizoguchi, T. Ujike and Y. Tominaga, *J. Chem. Phys.*, 1998, **109**, 1867–1872.
77 G. E. Walrafen, M. R. Fisher, M. S. Hokmabadi and W. H. Yang, *J. Chem. Phys.*, 1986, **85**, 6970–6982.
78 G. E. Walrafen, Y. C. Chu and G. J. Piermarini, *J. Phys. Chem.*, 1996, **100**, 10363–10372.
79 S. Bratos and R. M. Pick, *Vibrational spectroscopy of molecular liquids and solids*, Plenum Press, New York, 1980.
80 I. Ohmine and H. Tanaka, *Chem. Rev.*, 1993, **93**, 2545–2566.
81 M. Sasai, I. Ohmine and R. Ramaswamy, *J. Chem. Phys.*, 1992, **96**, 3045–3053.
82 C. P. Lawrence and J. L. Skinner, *Chem. Phys. Lett.*, 2003, **369**, 472–477.
83 A. Luzar, *J. Chem. Phys.*, 2000, **113**, 10663–10675.
84 D. C. Elton and M. Fernandez-Serra, *Nat. Commun.*, 2016, **7**, 1–8.
85 J. H. Wang, *J. Phys. Chem.*, 1965, **69**, 4412.
86 A. Oleinikova, I. Brovchenko, A. Geiger and B. Guillot, *J. Chem. Phys.*, 2002, **117**, 3296–3304.
87 H. E. Stanley, S. V. Buldyrev, M. Canpolat, O. Mishima, M. R. Sadr-Lahijany, A. Scala and F. W. Starr, *Phys. Chem. Chem. Phys.*, 2000, **2**, 1551–1558.
88 H. E. Stanley and J. Teixeira, *J. Chem. Phys.*, 1980, **73**, 3404–3422.
89 S. Alexander and R. Orbach, *J. Phys., Lett.*, 1982, **43**, L625–L631.
90 R. Rammal and G. Toulouse, *J. Phys., Lett.*, 1983, **44**, L13–L22.
91 C. T. Chudley and R. J. Elliott, *Proc. Phys. Soc., London*, 1961, **77**, 353–361.
92 L. van Hove, *Phys. Rev.*, 1954, **95**, 249–262.
93 G. H. Vineyard, *Phys. Rev.*, 1958, **110**, 999–1010.
94 C. Kittel, *Introduction to solid state physics*, Wiley, Hoboken, NJ, 8th edn, 2005.
95 R. Hilfer, *Physica A*, 1995, **221**, 89–96.
96 R. Hilfer, *Fractals*, 1995, **3**, 549–556.
97 I. I. Popov, R. R. Nigmatullin and A. A. Khamzin, *J. Non-Cryst. Solids*, 2012, **358**, 1516–1522.
98 A. A. Khamzin, R. R. Nigmatullin, I. I. Popov and B. A. Murzaliev, *Fract. Calc. Appl. Anal.*, 2013, **16**, 158–170.
99 A. Puzenko, Y. Hayashi, Y. E. Ryabov, I. Balin, Y. Feldman, U. Kaatze and R. Behrends, *J. Phys. Chem. B*, 2005, **109**, 6031–6035.
100 T. Head-Gordon and G. Hura, *Chem. Rev.*, 2002, **102**, 2651–2669.
101 C. J. F. Boettcher and P. Bordewijk, *Theory of Electric Polarization*, Elsevier, Amsterdam, 2nd edn, 1992.
102 A. A. Khamzin, I. I. Popov and R. R. Nigmatullin, *Phys. Rev. E: Stat., Nonlinear, Soft Matter Phys.*, 2014, **89**, 032303.
103 B. Roling, C. Martiny and S. Bruckner, *Phys. Rev. B: Condens. Matter Mater. Phys.*, 2001, **63**, 214203.
104 L. M. Zelenyi and A. V. Milovanov, *Phys.-Usp.*, 2004, **47**, 749–788.